The Journal of Chemical Physics

AIP Publishing

RESONANT AUGER DECAY OF DISSOCIATING CH_3I NEAR THE I 4d THRESHOLD

Stephen T. Pratt,[a]* Ugo Jacovella,[b] Bérenger Gans,[b] John D. Bozek,[c] and David M. P. Holland[d]

[a]Chemical Sciences and Engineering Division, Argonne National Laboratory, Lemont, IL 60439 USA

[b]Institut des Sciences Moléculaires d'Orsay, CNRS, Université Paris-Saclay, F-91405 Orsay, France

[c]Synchrotron SOLEIL, L'Orme des Merisiers, Départmentale 128, 91190 Saint-Aubin, France

[d]STFC, Daresbury Laboratory, Daresbury, Warrington, Cheshire, WA4 4AD, UK

*Corresponding Author Email: stpratt@anl.gov

ABSTRACT

Resonant Auger processes provides a unique perspective on electronic interactions and excited vibrational and electronic states of molecular ions. Here, new data are presented on the resonant Auger decay of excited CH_3I in the region just below the I $4d^{-1}$ ionization threshold. The resonances include Rydberg series converging to the five spin-orbit and ligand-field split CH_3I (I $4d^{-1}$) thresholds, as well as resonances corresponding to excitation from the I $4d_{5/2,3/2}$ orbitals into the σ* lowest unoccupied molecular orbital (LUMO). This study focuses on participator decay that populates the lowest lying states of CH_3I^+, in particular, the $\tilde{X}\ ^2E_{3/2}$ and $^2E_{1/2}$ states, and on spectator decay that populates the lowest-lying $(CH_3I^{2+})\sigma^*$ states of CH_3I^+. The CH_3I (I $4d^{-1}$)σ* resonances are broad, and dissociation to CH_3 + I competes with the autoionization of the core-excited states. Auger decay as the molecule dissociates produces a photoelectron spectrum with a long progression (up to $\nu_3^+ \sim 25$) in the C-I stretching mode of the $\tilde{X}\ ^2E_{3/2}$ and $^2E_{1/2}$ states, providing insight into the shape of the dissociative core-excited surface. The observed spectator decay processes indicate that the CH_3I^+ is formed on the repulsive wall of the lower-lying $(CH_3I^{2+})\sigma^*$ potentials, and the photon-energy dependence of the processes provides insight into the relative slopes of the $(4d^{-1})\sigma^*$ and $(CH_3I^{2+})\sigma^*$ potential surfaces. Data are also presented for the spectator decay of higher lying CH_3I (I $4d^{-1}$)*nl* Rydberg resonances. Photoelectron angular distributions for the resonant Auger processes provide additional information that helps distinguish these processes from the direct ionization signal.

Keywords: methyl iodide, photoelectron spectroscopy, resonant Auger Decay, ultrafast dissociation

I. INTRODUCTION

Resonant excitation of states lying just below the inner-shell ionization thresholds results in atomic and molecular decay processes that can involve fluorescence, autoionization, and dissociation.[1,2,3] When two or more of these processes occur on the same timescale, their competition can provide important insight into their dynamics and mechanisms.[1,2,3,4,5,6,7,8,9] The ability to excite particular resonant states selectively and correlate the observed decay processes with the character of the resonance can provide a deep understanding of the decay mechanisms. In addition, these processes often populate excited vibrational and electronic states of molecular ions that are difficult to populate directly, providing valuable insight into the structure of these species.

One particularly interesting situation arises when the dissociation lifetime is on the same timescale as the resonant Auger decay time. First observations of this "ultrafast dissociation" involved the decay of core-excited fragments produced by the dissociation of core-excited parent molecules.[10,11] In particular, Morin and Nenner[11] characterized the dissociation and autoionization of core-excited HBr in which a Br 3d electron was promoted to the antibonding σ* lowest unoccupied molecular orbital (LUMO). Photoelectron spectra showed clear evidence for dissociation to H + core-excited Br, followed by autoionization of the fragment Br atom. Numerous studies have since been performed on vibrational effects in Auger decay,[4,5,6,7,8,9,10,11,12] in particular, when this decay occurs as the core-excited molecule is dissociating.[3] Such processes typically produce a long tail on the vibrational distributions in the photoelectron spectra, which result from decay of the dissociating resonant state into high vibrational levels of the parent cation. Travnikova et al.[13] have also discussed multistep ultrafast dissociation following excitation of the HCl $1s^{-1}\sigma^*$ resonance, and how detuning across the resonance allows some control over the fragmentation dynamics.

In this paper, we extend our earlier work[14] on CH_3I and present new results on the Auger decay of resonances lying just below the I $4d_{5/2,3/2}^{-1}$ thresholds. The higher energy resonances are sharp and correspond to transitions from the two spin-orbit components of the I(4d) shell into the 6p, 5d, and

4f Rydberg states. The two lowest energy resonances correspond to excitation from the same initial orbitals into the antibonding σ* LUMO. These two resonances are quite broad (FWHM ~ 0.75 eV), and are analogous to the 3d → σ* resonance of HBr in the original ultrafast dissociation study of Morin and Nenner.[11] Although we do not observe the decay of free, core-excited I produced by ultrafast dissociation, the photoelectron spectra from participator Auger decay to the $\widetilde{X}\ ^2E_{3/2}$ and $^2E_{3/2}$ states of CH_3I^+ show very long progressions in the corresponding ν_3^+ C-I stretching vibration. The photoelectron angular distributions provide additional evidence for this long progression. We compare these results to the resonance Raman,[15,16] two-photon ionization,[17] and time-resolved pump-probe studies of the UV photodissociation of CH_3I via the corresponding valence-excited σ* LUMO,[18,19,20] which show similar dynamics of the dissociating molecule.

We also observe the spectator Auger decay processes of the CH_3I (I $4d^{-1}$)*nl* resonances into two-hole one particle states. The lowest energy states of this type lie in the region of the (single-hole) $\widetilde{B}\ ^2E$ state of CH_3I^+. The intensities of the spectator processes provide additional information on the nature of the decay processes.

II. EXPERIMENT

The experiments were performed at the PLEIADES undulator beamline of the Synchrotron SOLEIL.[21] This beamline is designed for soft x-ray studies and is equipped with a high-resolution VG Scienta R4000 electron spectrometer. The details of the undulator, beamline, and end station have been described previously.[21] Furthermore, the experimental approach for the present study near the I 4d thresholds of CH_3I is essentially the same as in our previous study.[14] Thus, only a few relevant details are discussed here.

The vapor from a room temperature CH_3I sample was introduced into a differentially pumped gas cell, and the pressure was controlled by a leak valve. All of the spectra were recorded within a small range of photon energies (50 – 60 eV), and the photon energy was calibrated by using the

spectrum of atomic Ne in the same energy range.[22,23] The ion yield scan of CH_3I between 50 and 60 eV recorded by measuring the total ion signal and normalizing by the photon flux is shown in Figure 1. The peak energies are given in Table 1. Photon energy scans of the Ne and CH_3I spectra

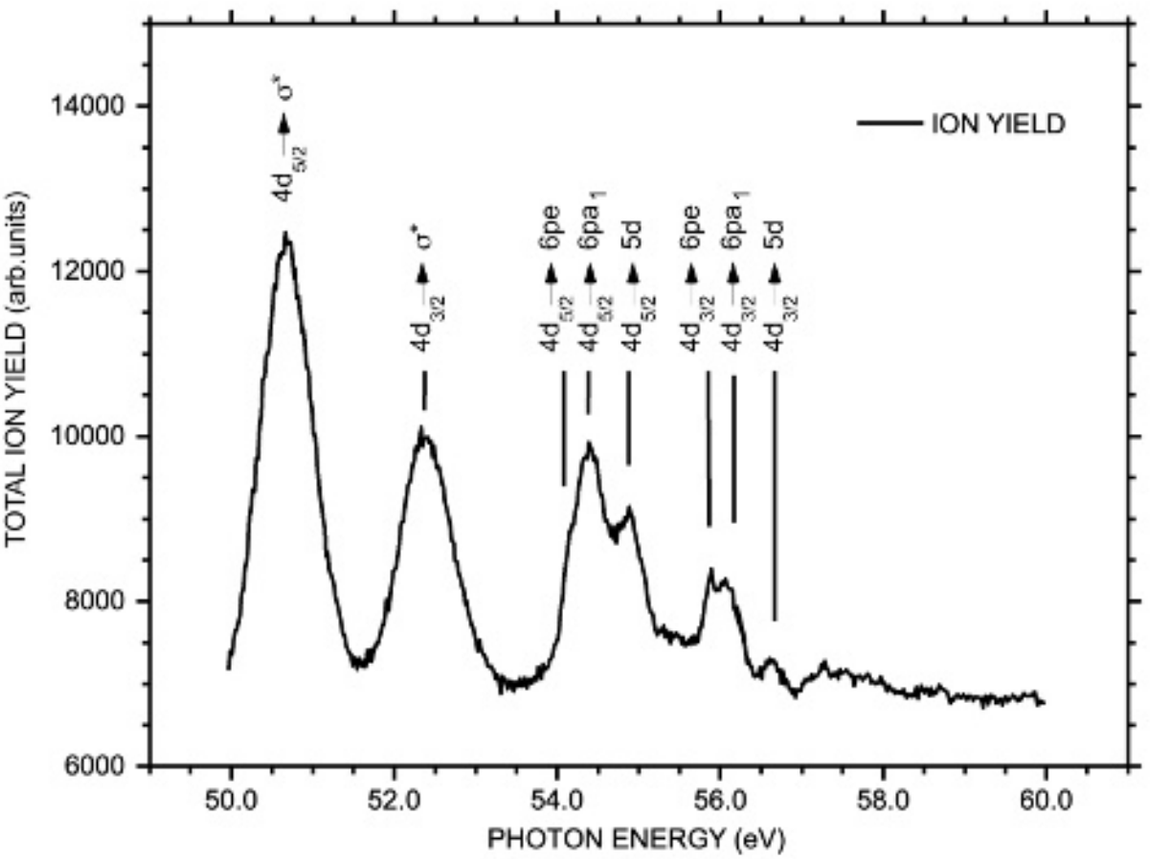

Figure 1. The total ion yield from CH_3I in the region of the I $4d^{-1}$ ionization thresholds. The ion signal has been divided by the photon signal to account for the changing photon flux in this energy range.

were reproducible to better than 3 - 5 meV. Once the photon energies were calibrated, the electron kinetic energies were calibrated by using the known ionization energy to produce the CH_3I^+ $\tilde{X}\,^2E_{3/2}$ ground state.[24] The calibration of the long progressions in the present electron spectra of the $\tilde{X}\,^2E_{3/2}$ and $^2E_{1/2}$ states was checked by comparison with the two-photon, zero electron kinetic energy spectra of Strobel et al.,[17] and the calibration appears to be good to within 2 – 4 meV. Off-

resonance spectra were recorded at energies close to the resonances to minimize any calibration issues with tuning the photon energy.

Table 1. Transition Energies from the 4d shell of CH_3I (eV).

Upper State	Energy (present)	Energy (Ref. 14)
$(4d_{5/2}^{-1})\sigma^*$	50.68	50.62
$(4d_{3/2}^{-1})\sigma^*$	52.39	52.34
$(4d_{5/2}^{-1})6pe$	54.18	54.10
$(4d_{5/2}^{-1})6pa_1$	54.38	54.33
$(4d_{5/2}^{-1})5d$	54.88	54.85
$(4d_{5/2}^{-1})4f$		55.56
$(4d_{3/2}^{-1})6pe$	55.88	55.86
$(4d_{3/2}^{-1})6pa_1$	56.10	56.09
$(4d_{3/2}^{-1})5d$	56.63	56.61
CH_3I^+ thresholds[(a)]		
$^2D_{5/2}$ $E_{1/2}$ ($\Delta_{5/2}$)		56.515 ± 0.02
$E_{3/2}$ ($\Pi_{3/2}$)		56.700 ± 0.02
$E_{1/2}$ ($\Sigma_{1/2}$)		56.870 ± 0.02
$^2D_{3/2}$ $E_{3/2}$ ($\Delta_{3/2}$)		58.242 ± 0.02
$E_{1/2}$ ($\Pi_{1/2}$)		58.446 ± 0.02

(a) The labels for the CH_3I^+ states are those for C_{3v} ($D_{\infty h}$) symmetry.

The electron intensities were not corrected for the electron kinetic energy dependence of the electron spectrometer transmission. This correction is expected to be small over the range of

kinetic energies sampled in the experiment. The photoelectron spectra were recorded with the linear polarization of the undulator light either parallel (0°) or perpendicular (90°) to the detection axis of the electron spectrometer. Within the electric dipole approximation, the angular distribution for the photoelectrons and Auger electrons is given by:[25,26,27]

$$\frac{d\sigma}{d\Omega} = \frac{\sigma}{4\pi}[1 + \beta P_2(\cos\theta)] \quad , \qquad (1)$$

where σ is the angle-integrated cross section, β is the angular distribution parameter, $P_2(\cos\theta) = (3\cos^2\theta\text{-}1)/2$, and θ is the angle between the polarization axis of the light and the detection axis of the electron spectrometer. Using the electron intensities at 0° and 90°, the value of β is given by:[28]

$$\beta = \frac{2(I_0 - I_{90})}{(I_0 + 2I_{90})} \quad , \qquad (2)$$

and the total cross section ("magic-angle" photoelectron spectrum) is proportional to:

$$\sigma \propto \frac{(I_0 + 2I_{90})}{3} \quad . \qquad (3)$$

For the photoelectron angular distributions, the electron signals at 0° and 90° were scaled by using an average value of the relative photon fluxes for the two undulator polarizations. The error bars on the β values due to counting statistics are typically less than ±0.05, although they can increase to as much as ±0.10 in regions of low photoelectron intensity. The resulting β values for the vibrationless $\tilde{X}\ ^2E_{3/2}$ and $^2E_{1/2}$ photoelectron peaks are approximately 0.1 – 0.2 lower than the previously reported values of Carlson et al.[29]

III. BACKGROUND

The removal of an I 4d electron from CH_3I results in two groups of states associated with the 4d $^2D_{5/2}$ and $^2D_{3/2}$ thresholds. The former group is lower in energy and splits into three states corresponding to $^2E_{1/2}(^2\Delta_{5/2})$, $^2E_{3/2}(^2\Pi_{3/2})$, and $^2E_{1/2}(^2\Sigma_{1/2})$, where the labels are for $C_{3v}(D_{\infty h})$ symmetry.[14,30] The higher energy $^2D_{3/2}$ group corresponds to a pair of states, $^2E_{3/2}(^2\Delta_{3/2})$ and $^2E_{1/2}(^2\Pi_{1/2})$.[30] The splitting between the two groups of states is ~1.65 eV, while the splittings within each group are on the order of 0.2 eV. As a result, in what follows the states within each group are

frequently lumped together as CH_3I^+ $4d_{5/2}^{-1}$ and $4d_{3/2}^{-1}$. The energies of all of these states are also given in Table 1.

The σ* resonances in Figure 1 correspond to these two groups of states of CH_3I^+ with an additional electron in the σ* LUMO. Of course, resonance states can be constructed as singlet or triplet combinations of the σ* electron with any of the five substates associated with ionization from the 4d shell. While two resonances are observed in Figure 1, there is no obvious evidence for multiple states contributing to either resonance, as the resonance widths are considerably larger than the splittings within each group of states. Nevertheless, multiple states are expected to contribute to each of the two σ* resonances. All of these states are expected to be strongly dissociative, and excitation from the groundstate equilibrium geometry of CH_3I is expected to access the repulsive wall of the σ* states. Classically, if there is a splitting between different states within the resonance, excitation at a given photon energy will access the different states at slightly different geometries of the molecule, e.g., slightly different C-I bond lengths, with intensities proportional to the square of the ground state vibrational wavefunction at that geometry.

Resonant Auger decay of core-excited molecules is a form of autoionization, and its mechanism can be divided into two types of processes: participator decay and spectator decay.[1,2] These are illustrated schematically in Figure 2. In participator processes, the excited electron is involved in the decay process, and the final state accessed is typically a one-hole state of the cation. In spectator processes, the core has sufficient energy of its own to decay without the involvement of the excited electron. Such processes generally result in two-hole, one-particle states. The excited electron in resonant Auger processes has a higher principal quantum number than the valence electrons, and thus its wavefunction has less amplitude at the short range necessary for the interactions that drive the decay. As a result, participator processes are generally slower than spectator processes, which involve only valence electrons. Of course, these are multi-electron processes, and relaxation results in the breakdown of the independent electron picture. Indeed, it is not always even possible to

separate the excitation and decay steps in the resonant Auger process, particularly when the excitation and detection bandwidths are narrower than the homogeneous linewidth of the intermediate state.[1,31]

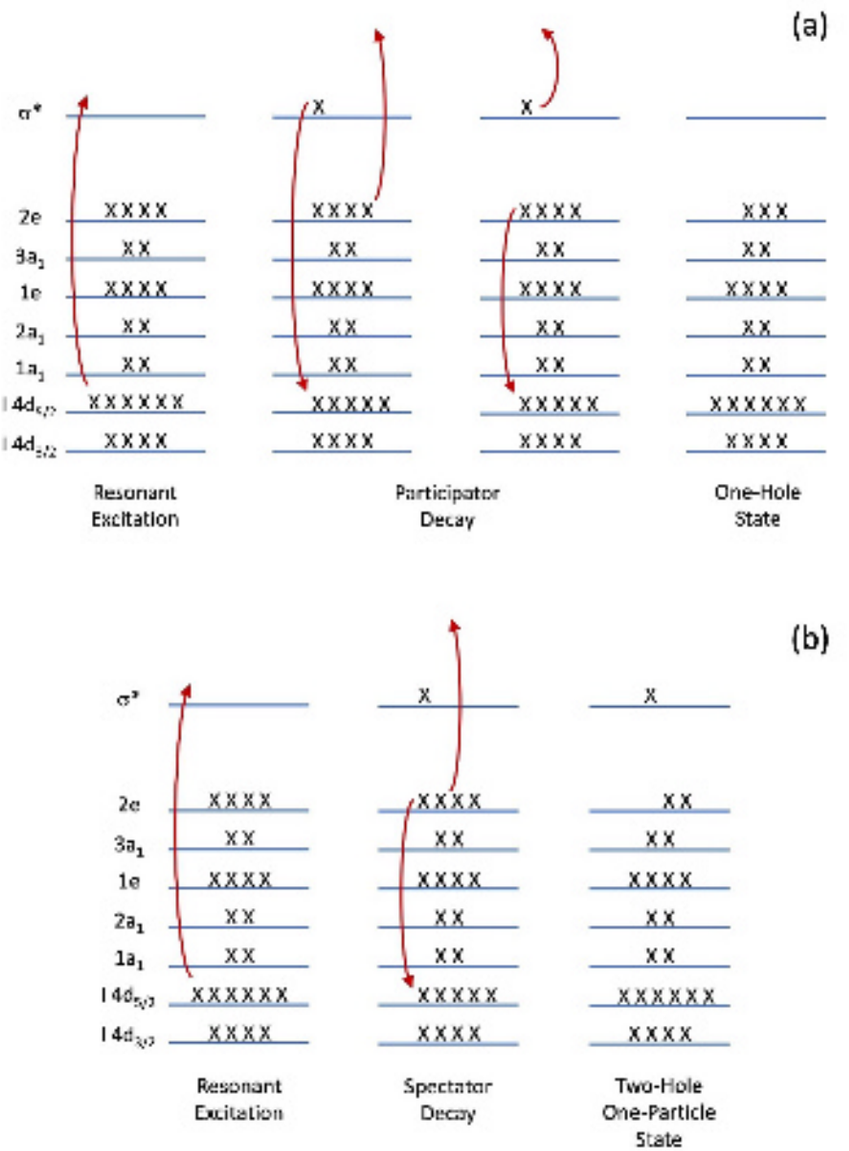

Figure 2. Schematic diagrams illustrating: (a) the participator and (b) spectator Auger decay processes following resonant I 4d excitation in CH_3I.

To simplify the analysis and discussion, here we focus primarily on the participator and spectator Auger processes that populate the lowest energy single-hole states and two-hole, one-particle states of CH_3I^+ respectively. For the participator processes, this choice corresponds to decay to the CH_3I^+ $\tilde{X}\ ^2E_{3/2}$ and $^2E_{1/2}$ states, which have energies of 9.53827 eV[24] and 10.1641 eV.[17] For the spectator processes, this choice corresponds to decay into the lowest $(CH_3I^{2+})\sigma^*$ states. Pilcher-Clayton and Eland[32,33,34] have performed photoelectron-photoelectron coincidence experiments to characterize the lowest electronic states of CH_3I^{2+}, and Pernpointner et al.[35] have performed theoretical calculations for these states. The lowest energy states of CH_3I^{2+} are given in Table 2. The double

Table 2. Lowest-Lying States of CH_3I^{2+} (eV).

State		Energy Exp.[(a)]	Energy Theo.[(b)]
$^3A_2$	A_1	26.664	25.82
	E	26.846	26.00
^1E		27.656	26.95
$^1A_1$		28.679	27.99

(a) The experimental energies are from Reference 32.
(b) The theoretical energies are from Reference 35.

ionization threshold of CH_3I to the CH_3I^{2+} $\tilde{X}\ ^3A_2$ ground state is 26.7 eV,[32] indicating the CH_3I^+ $\tilde{X}\ ^2E_{3/2} \rightarrow CH_3I^{2+}$ $\tilde{X}\ ^3A_2$ threshold is at 17.2 eV.

IV. RESULTS AND DISCUSSION

A. Participator Auger Decay to the CH_3I^+ $\tilde{X}\ ^2E_{3/2}$ and $^2E_{1/2}$ states

The wavelength scan shown in Figure 1 has a continuum background that is somewhat more intense than the resonant structure. This continuum results from direct photoionization from the lower energy valence-shell orbitals. Indeed, between 50 and 60 eV, the present photoelectron spectra recorded off resonance are very similar to those recorded at lower photon energies.[36,37]

On resonance, participator Auger processes can populate the same valence states accessed by direct photoionization. As an electronic autoionization process, to a first approximation the final state vibrational branching fractions for participator decay are determined by the Franck-Condon factors between the resonant state and the final electronic state of the cation.[38] While the valence-shell potential energy surfaces of CH_3I^+ are fairly well characterized,[39] those for the CH_3I (I $4d^{-1}$) core-excited states are less well known. The Rydberg states just below the I $4d_{5/2,3/2}^{-1}$ thresholds are expected to have potential surfaces similar to those of the corresponding cations. In contrast, based on their large linewidths and the antibonding character of the σ* orbital, the two broad $(4d^{-1})\sigma^*$ resonance states in Figure 1 are expected to be purely repulsive. Thus, the decay of these resonances will probe the competition between concurrent bond dissociation and Auger decay of the I 4d hole. While most of the excited valence states of CH_3I^+ are dissociative or predissociative, Figure 3 shows the $\tilde{X}\ ^2E_{3/2}$ and $^2E_{1/2}$ states are bound,[39,40] with dissociation energies of 2.713 ± 0.004 eV and 2.087 ± 0.004 eV, respectively.[17,41]

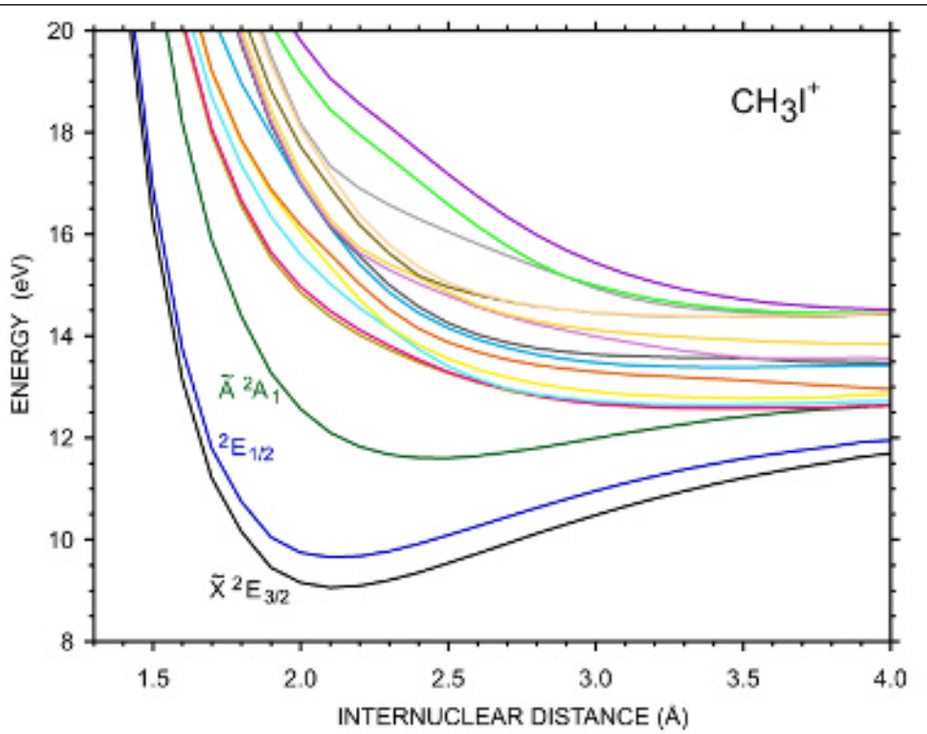

Figure 3. Cuts through the potential energy surfaces of CH_3I^+ along the C-I stretching coordinate in the energy region relevant to the present experiments. These curves are from the calculations of Murillo-Sánchez et al. (Reference 39).

Figure 4 shows the magic-angle photoelectron spectra for photon energies of 50.224 eV, off resonance, and 50.824 eV, on the (I $4d_{5/2}^{-1}$)σ* resonance. At first glance, the two spectra are quite similar, with the only obvious differences within the $\widetilde{B}$ state bands and at binding energies above 20 eV. (The latter are seen more clearly in Section IV.C.) As discussed below, these more obvious differences result from spectator Auger processes, which are generally stronger than participator processes.

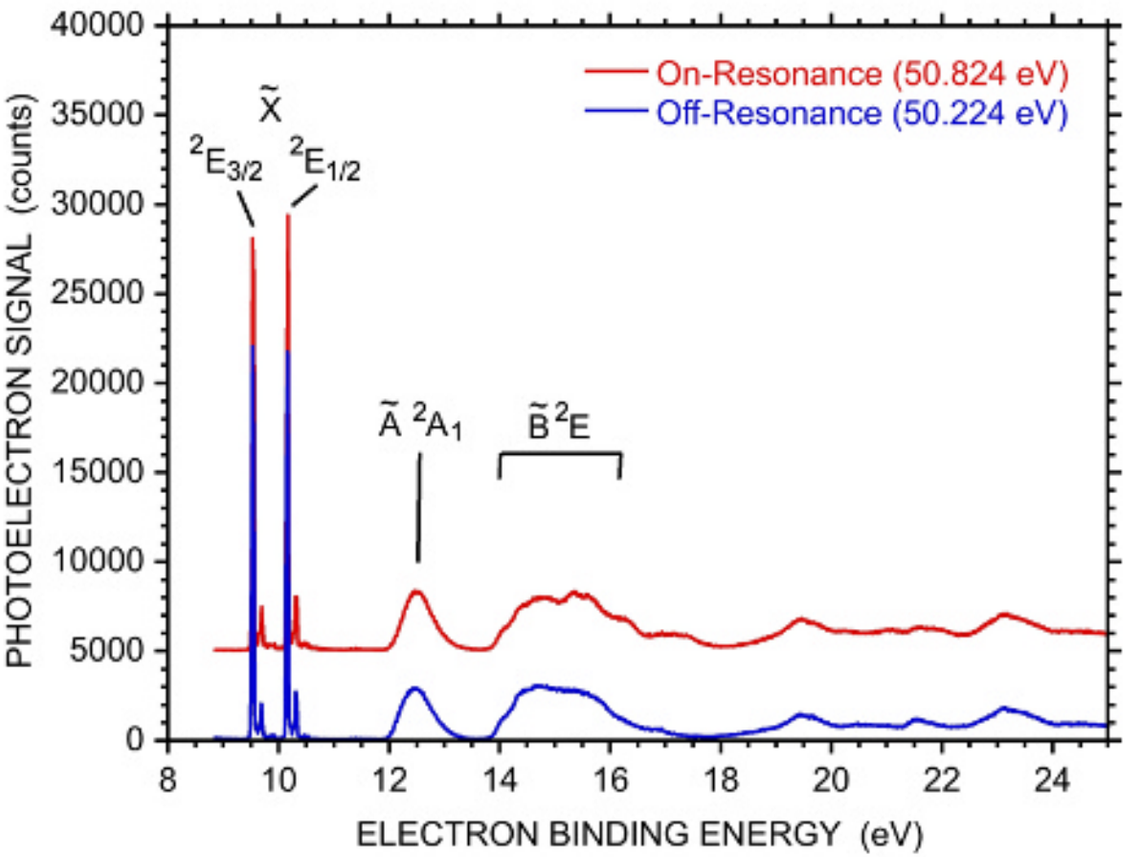

Figure 4. The magic-angle photoelectron spectrum determined by using the $\theta = 0^o$ and 90^o photoelectron spectra at a photon energy of 50.824 eV on the CH_3I ($4d_{5/2}^{-1}$)σ* resonance and off resonance at 50.224 eV. The spectra are plotted vs. electron binding energy.

Figure 5 shows a closer examination of the two lowest energy photoelectron bands, corresponding to ionization to the CH_3I^+ $\widetilde{X}$ $^2E_{3/2}$ and $^2E_{1/2}$ states. For this figure, the off-resonance spectrum at 51.574 eV is compared with the spectrum at 50.674 eV, on the (I $4d_{5/2}^{-1}$)σ* resonance, and the

spectra have been accumulated for 67% longer than for those in Figure 4. A very weak hot band corresponding to excitation from the ν_3" = 1 level of the CH_3I ground state to the vibrationless level of the CH_3I^+ ground state can be observed at 9.472 eV. Figure 5b shows the difference spectrum of the on-resonance spectrum minus the off-resonance spectrum, where the spectra have been normalized to the integrated intensity of the $\tilde{X}\ ^2E_{3/2}$, $\nu^+ = 0$ band. Thus, any participator decay

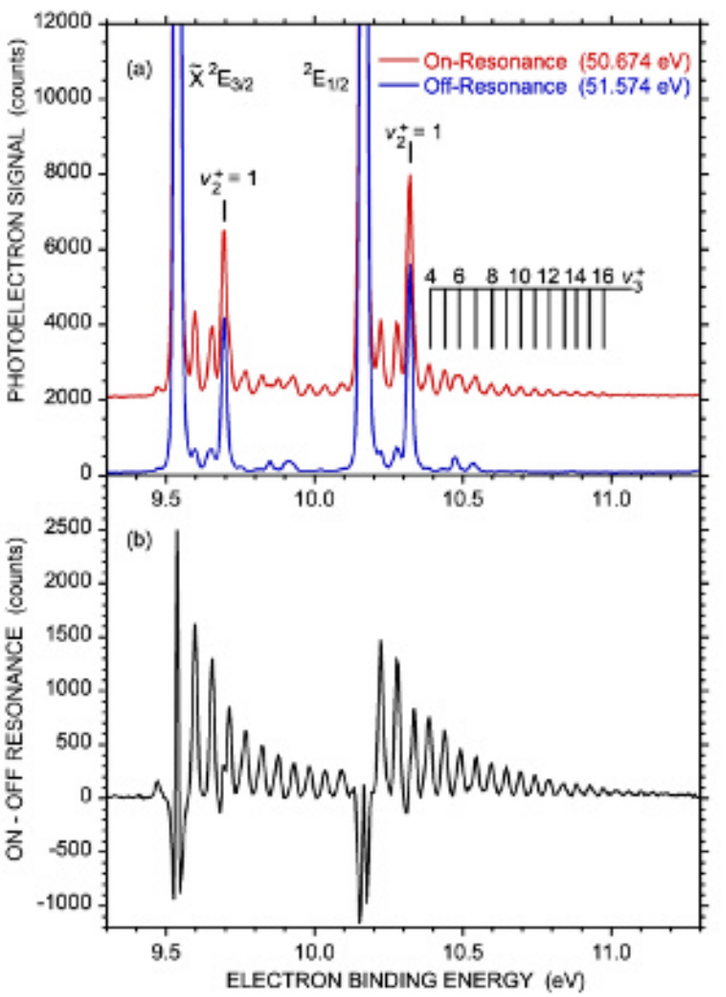

Figure 5. A portion of the magic angle photoelectron spectra determined from the $\theta = 0^o$ and 90^o spectra on-resonance (50.674 eV) and off-resonance (51.574 eV) for the transition to the (I $4d_{5/2}^{-1}$)σ^* resonance in the region of the CH_3I^+ $\tilde{X}\ ^2E_{3/2}$ and $^2E_{1/2}$ states. The spectra are plotted vs. electron binding energy and the on-resonance spectrum has been shifted up by 2000 counts for clarity. (b) The difference spectrum between the on- and off-resonance spectra of (a). The two spectra were normalized to the integrated intensity of the $\tilde{X}\ ^2E_{3/2}$ origin band, and the difference spectrum highlights the contribution from resonant participator Auger decay.

to the $\tilde{X}\ ^2E_{3/2}$, $v^+ = 0$ state will not be observed. The oscillatory lineshapes for the $\tilde{X}\ ^2E_{3/2}$, $v^+ = 0$ and $^2E_{1/2}$, $v^+ = 0$ peaks are a result of slightly different linewidths for the intense peaks in the on and off- resonance spectra. These differences are a result of small nonlinearities in the detector at high count rates.

Table 3. ν_3^+ Vibrational Levels of CH_3I^+ $\tilde{X}\ ^2E_{3/2}$ and $^2E_{1/2}$ (eV)[a]

v_3^+	$^2E_{3/2}$ (Ref. 17)	$^2E_{3/2}$ (Present)	$^2E_{1/2}$ (Present)
0	9.5381	9.538	10.165
1	9.5974	9.597	10.223
2	9.6556	9.655	10.279
3	9.7132	9.712[b]	10.334[b]
4	9.7696	9.767	10.386
5	9.8251	9.823	10.438
6	9.8802	9.877	10.491[c]
7	9.9342	9.929[c]	10.544
8	9.9875	9.983	10.595
9	10.0354	10.036	10.646
10	10.0871	10.092	10.694
11			10.742
12			10.789
13			10.837
14			10.884
15			10.929
16			10.973
17			11.017
18			11.057
19			11.101
20			11.139
21			11.183
22			11.231

(a) Energies are relative to the ground vibrational state of neutral CH_3I. The present experimental energies were determined by fitting a Gaussian function to the individual peaks.
(b) This peak is a shoulder on a much more intense vibrational band. The overlapped peaks were fit using a sum of two Gaussian functions.
(c) This peak is blended with another vibrational band.

In principle, the direct photoionization process and the participator autoionization process can interfere to produce Fano lineshapes.[42] Such interference would make the simple subtraction of the on- and off-resonance processes impossible. However, in the present case, the direct process to produce the high vibrational levels of the ν_3^+ C-I stretch is essentially negligible, thus allowing the simple off-resonance subtraction. Based on the intensities of the ν_3^+ bands, however, this contribution is expected to be no more than a few percent of the principal photoelectron peak. The negative-going features for the strongest peaks result from slight shifts in the energy axis and small differences in the electron spectrometer resolution.

The on-resonance and difference spectra in Figure 5 show a very long progression in the ν_3^+ C-I stretching vibration for both the $\widetilde{X}\ ^2E_{3/2}$ and $^2E_{1/2}$ states, although higher members of the former progression are obscured by the stronger lower members of the $^2E_{1/2}$ progression. While the on-resonance spectrum shows the same few bands of the CH_3I^+ ν_2^+ umbrella motion and the ν_6^+ CH_3 rocking vibration as the off-resonance spectrum,[36,37] the long progression on resonance appears to be purely composed of the ν_3^+ C-I stretching vibration. (The $v_6^+ = 1$ band appears at 9.641 eV as a very weak shoulder on the low-energy side of the $v_2^+ = 2$ band.) The observed levels are given in Table 3. The long participator progression in ν_3^+ is observed for excitation energies across the resonance (50.408 – 51.158 eV), with the intensity of this progression tracking the intensity profile of the resonance.

Figure 6 shows the photoelectron angular distribution parameter, β, for the on-resonance spectrum, where the on-resonance photoelectron energy spectrum has been included to allow the association of β values to particular resonances. For each member of the $\widetilde{X}\ ^2E_{3/2}$ and $^2E_{1/2}$ progressions, the β value shows a significant increase, with on-resonance $\beta \sim 0.75 \pm 0.15$. The non-zero β values at energies above 11.1 eV result from the weak underlying continuum signal.

Spectra recorded across both the (I $4d_{5/2}^{-1}$)σ* and (I $4d_{3/2}^{-1}$)σ* resonances show similar behavior in the photoelectron spectra and β values. The long progressions for these two bands are interpreted as arising from the autoionization of the dissociative σ* resonances, and suggest that the potential surfaces are purely repulsive along the C-I reaction coordinate, and the absence of bands for other vibrational modes indicates that energy is not diverted into vibrational coordinates perpendicular to the reaction coordinate.

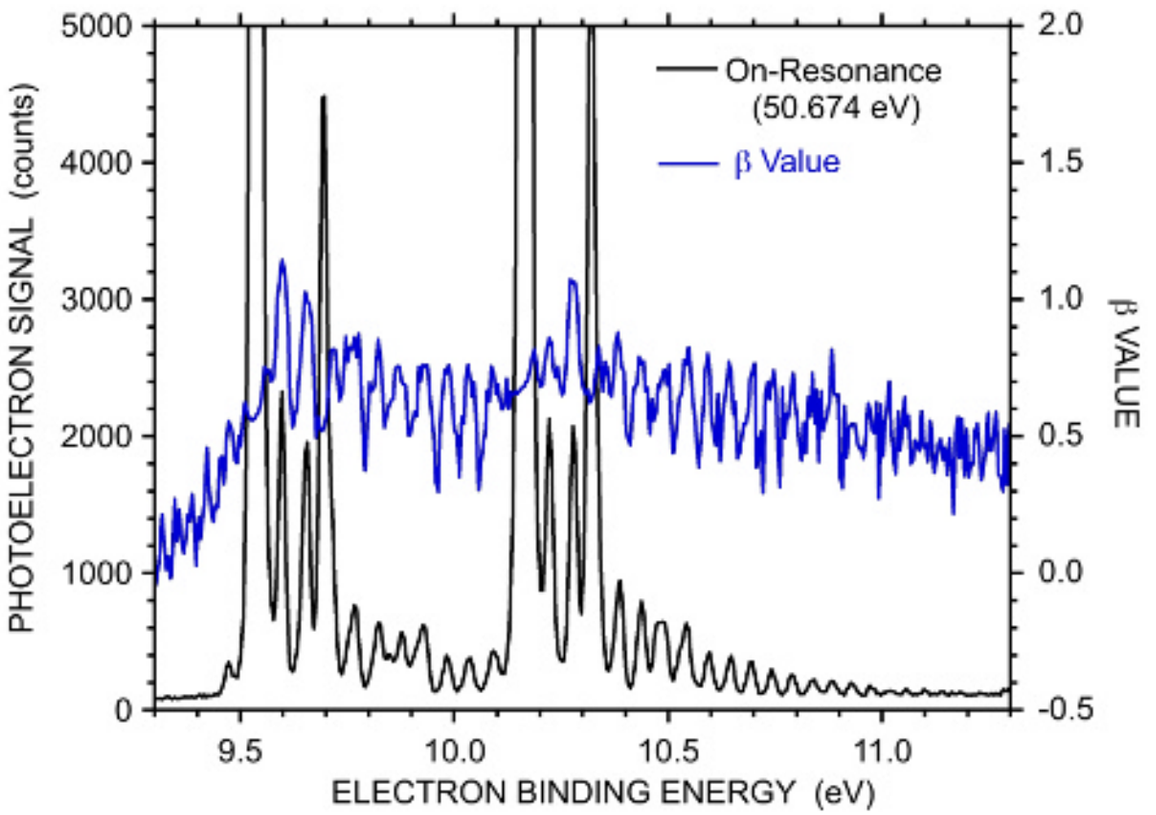

Figure 6. The magic angle photoelectron spectrum determined from the $\theta = 0^o$ and 90^o spectra on-resonance (50.674 eV) photoelectron spectra, along with the corresponding photoelectron angular distribution parameter, β.

It is interesting to compare the excitation of CH_3I from the I 4d shell into the σ* LUMO with excitation from the CH_3I HOMO into the "same" σ* LUMO. Of course, the LUMO in the presence of the $\tilde{X}\,^2E_{3/2}$ core is different from that in the presence of the CH_3I^+ (I $4d_{5/2,3/2}^{-1}$) core. Nevertheless,

both excited states are strongly dissociative. Excitation from the CH_3I HOMO into the LUMO is a benchmark system for photodissociation studies,[43,44] including some recent work using high-harmonic generation[18,19] and free-electron laser[20] probes with site-specific excitation to monitor the dissociation process. The dissociation process actually involves several interacting electronic states, but the oscillator strength is primarily carried by just one of these. Perhaps most relevant to the present study are resonance Raman[15] and emission studies[45] of the dissociation process, as well as zero-kinetic energy (ZEKE) photoelectron spectroscopy following two-photon ionization via the dissociating σ* state.[17] Resonance Raman[15] and fluorescence[45] data for the σ* resonance near 266 nm show long progressions in the C-I stretch of the neutral CH_3I $\tilde{X}\ ^1A_1$ final state, but this progression was extended only to $\sim\nu_3'' = 12$. Significant intensity is also observed in other vibrational modes, including the ν_1'' CH_3 symmetric stretch. Similarly, two-photon ZEKE spectra via this dissociative state show a long progression in ν_3^+, but this progression terminates at $\nu_3^+ \sim 10$.[17] In addition, the ZEKE spectrum[17] shows excitation of a number of different vibrational modes, including the CH_3 umbrella mode, ν_2^+, the asymmetric stretching mode, ν_4^+, and the CH_3 rocking mode, ν_6^+. While the vibronic intensities in ZEKE spectra are determined by a number of factors, the positions of the ZEKE peaks do reflect the corresponding ionization thresholds of the molecule, although they may need to be corrected for small electric field shifts. The present observation of excitation only in ν_3^+ suggests that the dissociation dynamics of the CH_3I (I $4d_{5/2,3/2}^{-1}$)σ* resonances are much simpler than those of the lower energy valence-excited state.

The long progression in the present C-I stretching vibration suggests that some CH_3I (I $4d^{-1}$)σ* molecules might fully dissociate before Auger decay occurs. In their original study of HBr, Morin and Nenner[11] excited the 3d → σ* transition, and observed autoionization from the atomic Br fragment. This (Br $3d^{-1}$)σ* state, which is analogous to the present CH_3I (I $4d^{-1}$)σ* states, dissociated to H + core-excited Br ($3d^9 4s^2 4p^6$) $^2D_{5/2,3/2}$ atoms, which were observed to autoionize to a number of levels of Br^+. Note that in the excited state dissociation process, the 3d or 4d holes are assumed to remain on the halogen atom throughout the dissociation process. Assuming the

CH_3I (I $4d^{-1}$)σ* resonances dissociate to the corresponding CH_3 + I ($4d^9 5s^2 5p^6$) $^2D_{5/2,3/2}$ fragments with the known atomic I excitation energies of 45.87 eV and 47.63 eV,[46] respectively, the expected energies for autoionization of the I fragments can be calculated. These energies are given in Table S1 of the Supplemental Material. Comparison with the present experimental data shows little evidence for atomic autoionization at the expected energies. It is possible that the ($4d^{-1}$)σ* resonances dissociate to lower energy levels of I that autoionize to produce slower electrons, but no evidence for such processes has been identified. Thus, it appears that the Auger decay occurs before the molecule is fully dissociated. The larger mass of the dissociation fragments results in their slower separation; thus, the molecules may all undergo Auger decay before dissociation is complete.

While the photoelectron spectra on the (I $4d_{5/2,3/2}^{-1}$)σ* resonances show very long progressions in the ν_3^+ C-I stretching vibration, examination of slices through the CH_3I^+ potential energy surfaces[39] indicates that even the $^2E_{1/2}$, ν_3^+ = 21 level is only a little more than halfway to the dissociation limit, and the corresponding outer turning point at this energy is only ~3.2 Å. Thus, as indicated above, autoionization of the σ* resonance must be fast enough to prevent dissociation into neutral fragments. One aspect of this ionization mechanism merits discussion. In the (I $4d_{5/2,3/2}$)σ* resonances, the positive charge of the CH_3I^+ core is primarily on the iodine atom. Similarly, the HOMO has predominately lone-pair character on the I atom,[37,47] so that the charge in the CH_3I^+ $\tilde{X}$ $^2E_{3/2,1/2}$ states is localized on the I atom. Thus, autoionization of the (I $4d_{5/2,3/2}$)σ* resonances to the $\tilde{X}$ $^2E_{3/2,1/2}$ states can occur in a straightforward fashion. However, at large C-I bond lengths, the $\tilde{X}$ $^2E_{3/2,1/2}$ states dissociate to CH_3^+ + I $^2P_{3/2}$, with the charge localized on the CH_3 radical. Since the hole remains on the I atom throughout dissociation on the (I $4d_{5/2,3/2}^{-1}$)σ* surface, this result requires charge transfer from the I atom to the CH_3 radical somewhere during the autoionization/dissociation process for the $\tilde{X}$ $^2E_{3/2,1/2}$ states.

The "over-the-barrier" model for charge transfer is often used to estimate the bond length at which charge transfer from the I to the CH_3 becomes classically forbidden. With this model, the critical distance, R_c(Å), is given by:[48,49,50,51]

$$R_C = 0.529\ \frac{(p+1) + 2\sqrt{(p+1)q}}{E_i} \quad , \qquad (4)$$

where p is the initial charge on the CH_3 (0), q is the initial charge on the I (+1), and E_i is the electron binding energy on the CH_3 in atomic units (0.36 a.u.). This yields a value of 4.4 Å, considerably larger than the outer turning point of the $^2E_{1/2}$, $v_3^+ = 21$ level, ~3.2 Å. Thus, this exercise again supports the idea that it is fast autoionization that restricts the dissociation to neutral fragments, rather than the influence of some other mechanism.

Participator Auger decay of the CH_3I (I $4d_{5/2,3/2}^{-1}$)σ* resonances can also populate higher energy states of CH_3I^+, for example, the states associated with the $\widetilde{A}$ and $\widetilde{B}$ bands of the photoelectron spectrum. In high-resolution photoelectron spectra,[36] the $\widetilde{A}$ band shows partially resolved vibrational structure involving several normal modes on top of a broad continuum. With the present resolution, this vibrational structure is not resolved. Comparison of the shape of the broad continuum of the $\widetilde{A}$ band in the on- and off-resonance spectra of Figure 4 shows only a very small change in the shape of the envelope that is difficult to quantify. Similar difficulties occur for the higher energy bands. While there are significant changes in the $\widetilde{B}$ band of the photoelectron spectra recorded on- and off-resonance, as discussed below, these changes are attributed to spectator Auger decay.

Finally, we consider participator Auger decay from the higher energy Rydberg states in Figure 1. The rate for the participator process depends on the probability for the excited electron to be at short range, where it can interact with the core electrons. This probability is expected to scale as $1/n^{*3}$, where n^* is the effective principal quantum number of the excited electron.[52] Using a spin-orbit averaged CH_3I $4d_{5/2}^{-1}$ ionization threshold, the n^* values for the CH_3I (I $4d_{5/2}^{-1}$)σ* and (I

$4d_{5/2}^{-1}$)6pe states are 1.504 and 2.326, respectively. Then, using the $1/n^{*3}$ scaling, the participator Auger process for the CH_3I (I $4d_{5/2}^{-1}$)6pe state is expected to be ~3.6 times slower than that for the CH_3I (I $4d_{5/2}^{-1}$)σ* state, with the higher Rydberg states being even slower. In contrast, the competing spectator decay processes involve only the core electrons, and should be essentially independent of n^*. Thus, compared to the already weak participator processes for the σ* states, the participator processes for the 6pe and higher Rydberg states are expected to be of nearly negligible importance. This conclusion is borne out by the present observations.

B. Spectator Auger Decay to the region of the CH_3I^+ $\widetilde{B}$ ^2E state

In the absence of orbital relaxation that can produce "shake" processes, spectator Auger decay of the CH_3I (I $4d_{5/2,3/2}^{-1}$)σ* resonances will lead to (CH_3I^{2+})σ* states based on the energetically accessible doubly charged states of CH_3I^{2+}. Of course, shake-up and shake-down processes can result in decay to other final states, but these are expected to be weaker than the primary decay process. A crude estimate of the binding energy of the lowest energy (CH_3I^{2+} $\widetilde{X}$ $^3A_2$)σ* state can be made as follows. The ionization energy of CH_3I is 9.53827 ± 0.00002 eV[24] and, using the term energy of the $\widetilde{A}$ state from Herzberg,[53] the binding energy of the σ* upper state of the HOMO-LUMO transition is ~6.067 eV. The lowest double ionization threshold of CH_3I is 26.664 eV,[32,35] yielding an ionization energy for CH_3I^+ $\widetilde{X}$ $^2E_{3/2}$ of 17.126 eV. In the hydrogenic approximation,[54] the latter ionization energy should be Z^2 (here, 2^2 vs. 1^2), or 4 times larger than the neutral ionization energy. Using the measured ionization energies, the effective value of Z^2 is only 17.126/9.538 = 1.80. Thus, the expected binding energy for the lowest energy (CH_3I^{2+} $\widetilde{X}$ $^3A_2$)σ* state is 10.92 eV (= 6.6067 x 1.8). This estimate would put the lowest energy (CH_3I^{2+} $\widetilde{X}$ $^3A_2$)σ* state at ~15.74 eV, within the $\widetilde{B}$ $^2E \leftarrow \widetilde{X}$ $^1A_1$ band of the photoelectron spectrum. Pilcher-Clayton and Eland[32] observed a number of double ionization features within 2 – 3 eV of the double ionization threshold, and this observation has been validated by theoretical calculations from Pernpointner et al.[35] Thus, multiple (CH_3I^{2+})σ* states are expected in the region of the $\widetilde{B}$ ^2E band. Indeed, Locht et al.[55] calculated vertical excitation energies to the three lowest (CH_3I^{2+})σ* states,

and found values of 15.22, 15.77, and 16.14 eV relative to the neutral ground state, consistent with our qualitative estimate. They also found a number of additional electronically excited σ* states of CH_3I^+ between 16.7 and 20.2 eV. As seen in Figure 3, the recent calculations of Murillo-Sánchez et al.[39] also show a number of repulsive states cutting through this region near the equilibrium geometry of the molecule. These states dissociate to CH_3 $\tilde{X}$ $^2A_2$" + I^+ $^3P_{2,1,0}$ or $^1D_2$, as well as to CH_3^+ $\tilde{X}$ $^1A_1$' + I $^2P_{1/2}$. González-Vázquez et al.[40] have recently performed more detailed calculations of the ionic potential curves in this region and, although these curves are still repulsive in the Franck-Condon region, some of them show metastable minima at larger C-I distances. This observation is not expected to affect the conclusions presented here.

In the He I photoelectron spectrum of CH_3I,[37] the $\tilde{B}$ ^2E band is produced by direct photoionization out of the 2e (HOMO-2) orbital. The corresponding single-hole state of CH_3I can also be produced by participator Auger decay of the $(4d^{-1})\sigma^*$ resonances although, as in the case of participator decay to the $\tilde{X}$ $^2E_{3/2,1/2}$ states, these processes are expected to be weak. In contrast, the two-hole, one-particle $(CH_3I^{2+})\sigma^*$ states are expected to be populated only weakly by direct photoionization, as this process requires a two-electron transition. However, spectator Auger processes via the $(4d^{-1})\sigma^*$ resonances provide a clear route to populate these two-hole, one-particle states. Note that core-relaxation can result in "shake" processes that excite or de-excite ("shake-up" or "shake-down" processes, respectively), the σ* electron into other orbitals.[1,2] However, the σ* orbital is relatively isolated: based on the positions of the resonances just below the I $4d^{-1}$ thresholds, the next possible unoccupied orbital is expected to lie ~3.5 eV higher in energy and should not appear in the region of the $\tilde{B}$ ^2E bands.

Excitation to the $(4d^{-1})\sigma^*$ states accesses points on the repulsive wall of the potential surfaces, and rapid spectator decay will access the repulsive walls of the potentials for the states in the region of the $\tilde{B}$ ^2E state. Thus, the decay process is a free-free transition with respect to the nuclear motion, and the kinetic energy spectrum of the ejected electrons will be continuous. This is shown

schematically in Figure 7. Classically, excitation at a given energy will access a specific point on the repulsive $(4d^{-1})\sigma^*$ potential, and instantaneous decay will access the lower potential surface at the same geometry of the molecule. Quantum mechanically, the excitation is spread out over a range of geometries in the excited state, and slower Auger decay will access a greater range of geometries on the final-state surface.

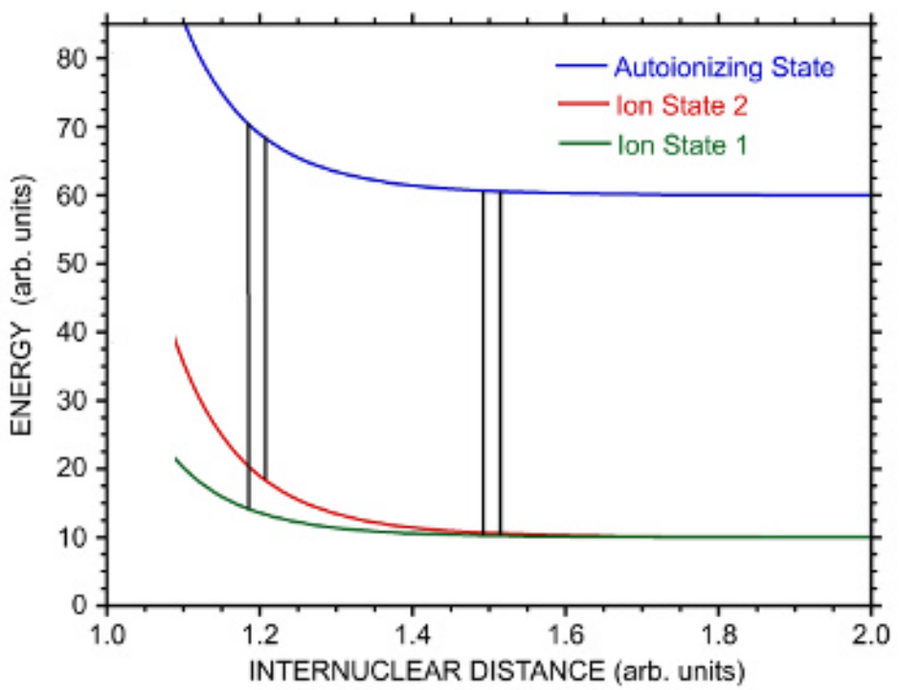

Figure 7. A schematic diagram of the potential curve for a neutral autoionizing state (blue) and two final-state ion curves (red and green curves) along the bond dissociation axis. State 2 is drawn parallel to that of the autoionizing state, while state 1 is considerably less repulsive. From a classical perspective, the excitation photon energy from the ground state neutral selects the internuclear distance at which the autoionizing curve is accessed, with higher energy photons accessing shorter bond lengths. The kinetic energy of the ejected electron is determined by the difference in energy between the autoionizing and ion states. For state 2, the electron kinetic energy is independent of internuclear distance, and the electron binding energy ($h\nu$ - E_{ke}) increases in step with the photon energy. For the more attractive potential of state 1, the electron kinetic energy increases with increasing photon energy, and the corresponding electron binding energy will increase more slowly than the photon energy.

Unlike photoionization to a discrete state, where the electron kinetic energy, E_{ke}, tracks the photon energy ($E_{ke} = h\nu - IE$), where IE is the corresponding ionization energy, and yields a constant

binding energy, the photon energy dependence of the electron kinetic energy for the continuum final state tracks the relative slopes of the repulsive $(4d^{-1})\sigma^*$ potentials and the repulsive $(CH_3I^{2+})\sigma^*$ potentials. If they are parallel, the electron kinetic energy will be constant with increasing photon energy, and thus the plotted binding energy will increase linearly with photon energy. If, however, the $(CH_3I^{2+})\sigma^*$ potential is not as steep as the $(4d^{-1})\sigma^*$ potential, the electron kinetic energy will increase faster with increasing photon energy, and the inferred binding energy

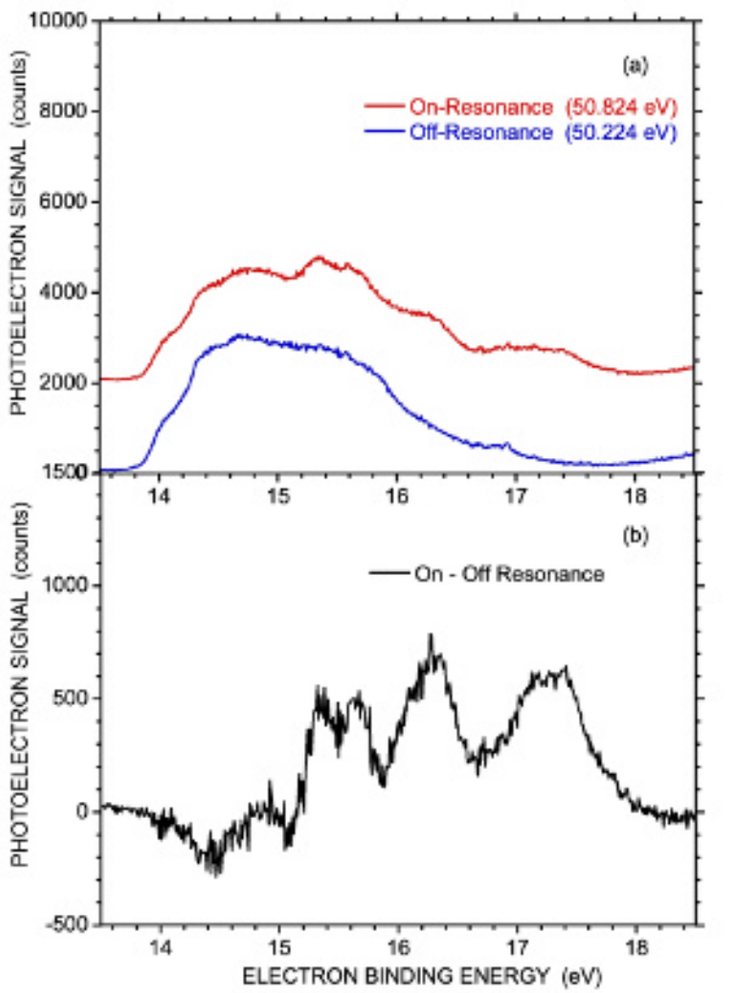

Figure 8. (a) The magic-angle photoelectron spectra of CH_3I determined from the $\theta = 0^o$ and 90^o spectra recorded on-resonance (50.824 eV) and off-resonance (50.224 eV). (b) The difference spectrum of the on- and off- resonance spectra of (a). The two spectra were normalized to each other on the leading edge of the band near 14.4 eV.

will increase at a slower rate than the photon energy. This behavior is also illustrated in Figure 7, and similar behavior has been discussed previously.[31]

As discussed above, the resonant photoelectron spectra recorded within the CH_3I (I $4d_{5/2,3/2}^{-1}$)σ* resonances do show significant features that are not observed in the off-resonance spectra, and these are now discussed in more detail.

Figure 8 shows the photoelectron spectrum of CH_3I in the region of the $\widetilde{B}$ state band at photon energies on (50.824 eV) and off (50.224 eV) the ($4d_{5/2}^{-1}$)σ* resonance. The spectra show small differences up to ~15.1 eV binding energy, and more substantial differences between 15.1 and 18 eV. The spectra in Figure 8 have been normalized to each other on the low-energy side of the band (14.1 eV), and the difference spectrum is also shown. As in the case of the participator decay processes, it is possible that the spectator decay process will interfere with the direct photoionization process,[42] thus making this simple subtraction of the on- and off-resonance spectra untenable. However, spectator processes tend to populate two-hole, one-particle final states, while direct photoionization tends to populate single-hole states, and thus interference is expected to be small for these processes. As a result, simple subtraction of the on- and off-resonance spectra can still be meaningful. Note, however, that configuration interaction between the single-hole states and the two-hole, one-particle states is possible, and that shake-up and shake-down processes can result in the same final states for the direct and indirect processes. Thus, interference effects may be important in some portions of the resonant Auger spectra.

Figure 9 shows a plot of the corresponding difference in β values (β_{on} - β_{off}) at the same two photon energies of Figure 8 (50.824 eV and 50.224 eV, respectively) and over the same range of electron binding energies. The on-resonant peaks due to spectator Auger decay are clearly associated with dips in the β value.

The small differences in the signal at lower energies within the band are likely due to participator Auger processes that produce small changes in the vibrational branching fractions for the photoionization process. Above 15.1 eV, the difference spectrum clearly displays broad features. These are considerably more intense than those for participator processes in the $\widetilde{X}\ ^2E_{3/2,\ 1/2}$ bands, and they are assigned to resonant spectator decay from the $(4d_{5/2}^{-1})\sigma^*$ resonance state of CH_3I to dissociative $(CH_3I^{2+})\sigma^*$ states of CH_3I^+. Similar features are observed in difference spectra across the resonance profile of the $(4d_{5/2}^{-1})\sigma^*$ and $(4d_{3/2}^{-1})\sigma^*$ resonances. Note, however, that none of the higher energy $4d^{-1}$ resonances in Figure 1 show any such additional structure within the $\widetilde{B}$ state band, reinforcing the conclusion that the structure arises from resonant spectator decay of the $(4d^{-1})\sigma^*$ resonances.

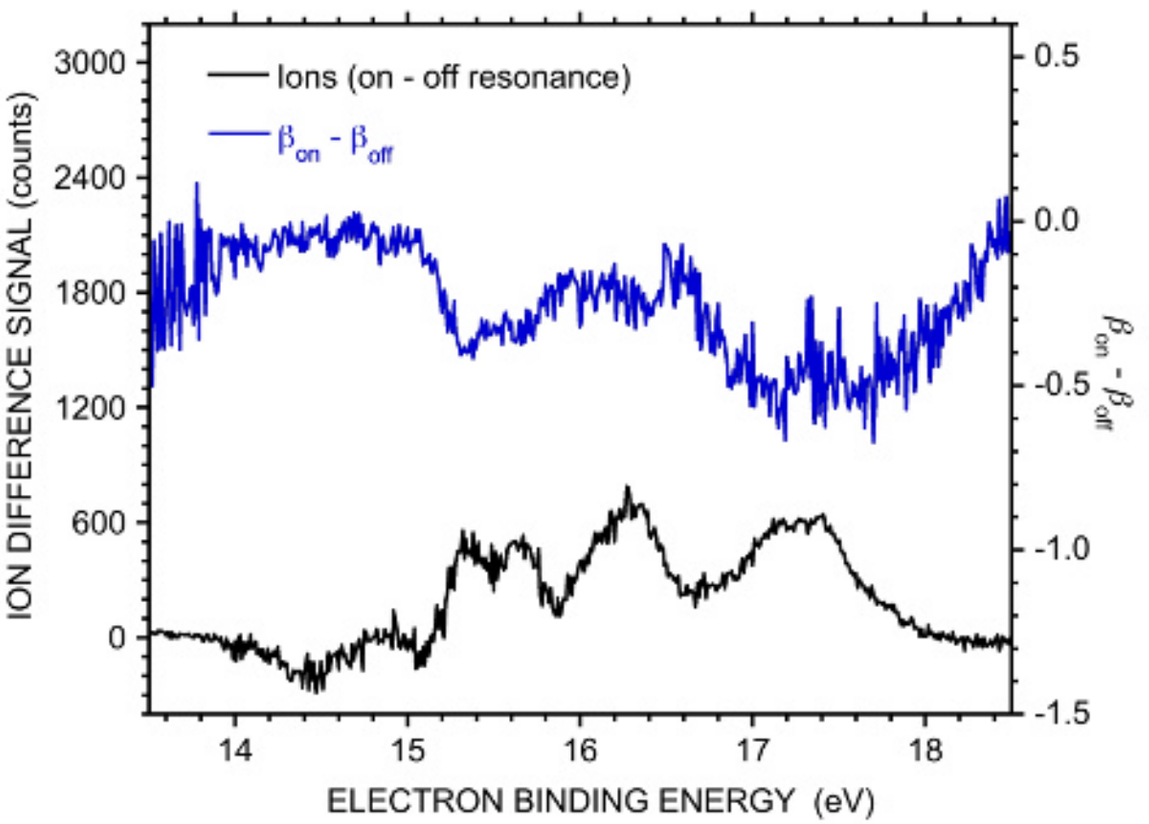

Figure 9. The difference spectrum of the on- and off- resonance magic-angle photoelectron spectra at 50.824 eV and 50.224 eV, respectively, along with the difference spectrum of the corresponding photoelectron angular distributions.

Figure 10 shows a series of on-resonance minus off-resonance spectra for the $(4d_{5/2}^{-1})\sigma^*$ resonance, and Figure 11 shows a similar series of spectra for the $(4d_{3/2}^{-1})\sigma^*$ resonance. A small air leak during the recording of the spectra in Figure 11 resulted in several sharp features from the photoionization of nitrogen and oxygen.[37] These features could be effectively removed from the

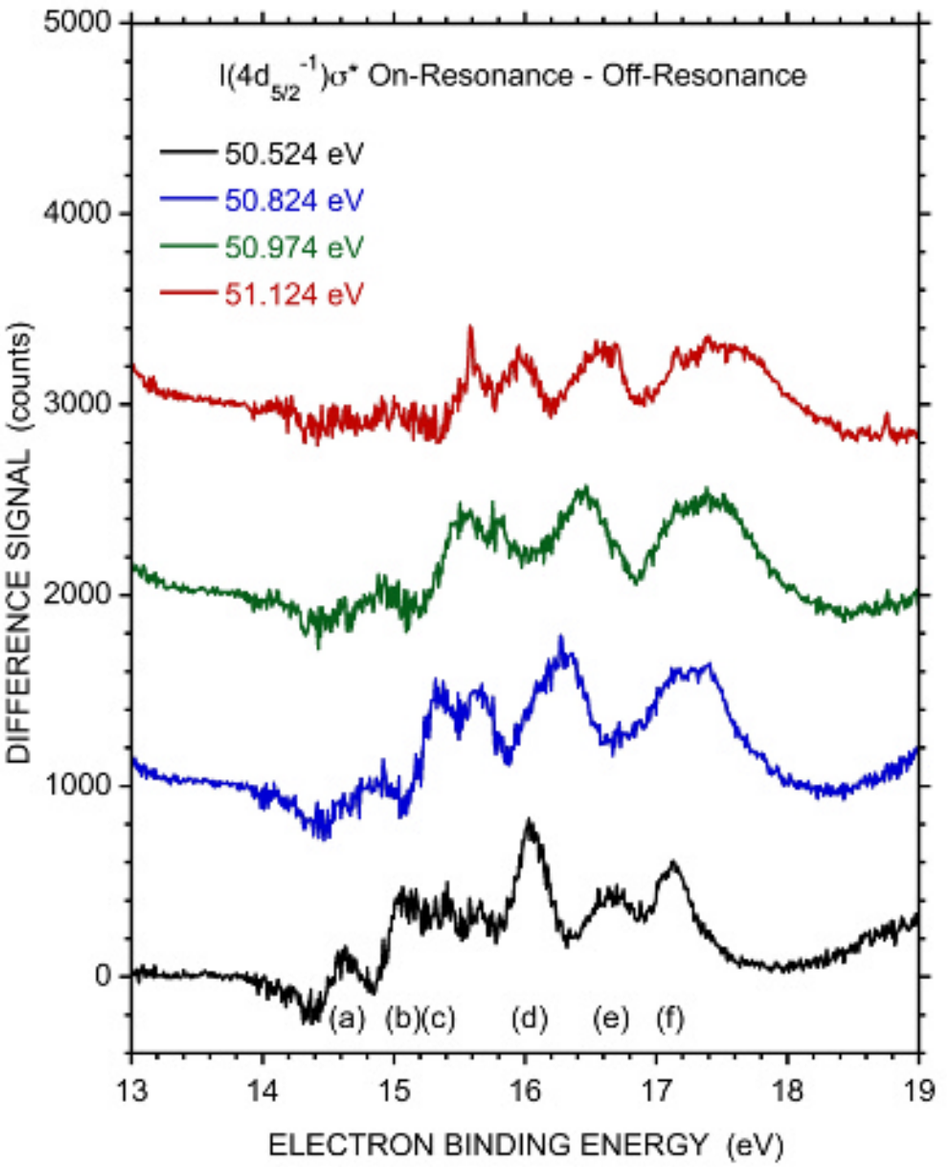

Figure 10. A series of difference magic-angle photoelectron spectra recorded at several energies across the (I $4d_{5/2}^{-1}$)σ^* resonance and using the off-resonance spectrum at 50.224 eV. The spectra have been scaled to the same peak intensity. The peaks are labeled (a) – (f) to facilitate comparison with Figure 11.

spectra in Figure 11 by using a linear combination of off-resonance spectra recorded before and after the scans of interest for the background subtraction. The impurity peaks occurred at constant binding energy as a function of photon energy, and were used to verify the calibration of the spectrum. Some of the spectra in Figure 10 also show weak sharp features that have the same source.

The difference spectra in Figure 10 show a series of peaks that move to higher binding energy with increasing photon energy. As in Figure 8, the lowest energy spectrum in Figure 10 shows weak structure below 15.0 eV that is assigned to participator Auger processes, while the substantial increase in signal at higher energies and the series of more intense peaks are due to spectator processes. The shifting of these peaks with increasing photon energy is reasonably straightforward to follow, although some of the peaks appear to merge or broaden at higher energy. This behavior is not surprising based on the potential curves along the C-I coordinate[39] shown in Figure 3, as these curves also merge and cross with increasing energy. In the binding energy range of the difference spectra, multiple dissociative states are calculated within the relevant span of internuclear distances. While the general assignment of the features in Figure 10 to spectator decay to (CH_3I^{2+}) σ* states is reasonable, the lack of knowledge of the ($4d^{-1}$)σ* potentials and limitations associated with the theoretical potentials of Figure 3 preclude a detailed assignment at this time.

Figure 11 is considerably simpler than Figure 10, as the difference spectra show only two significant features. Again, owing to the multiple possible final states, the specific assignments are not possible at this time. However, in both Figures 10 and 11, the photon energy dependence of the electron binding energies can be characterized in some detail. Figure 12 shows a plot of the electron binding energies of the observed peaks in Figures 10 and 11 as a function of the photon energy. Because the peak shapes are irregular, the positions were determined from the peak maxima. For Figure 10, some of the features show a smooth photon energy dependence, while others are more irregular, suggesting a curving or perturbation of the lower state surface. For

Figure 11, the two intense features labeled (d) and (f) show very smooth photon energy dependences. These two principal features may be associated with the same final states as the peaks labeled (d) and (f) in Figure 10, although the slopes in Figure 12 are somewhat different. At

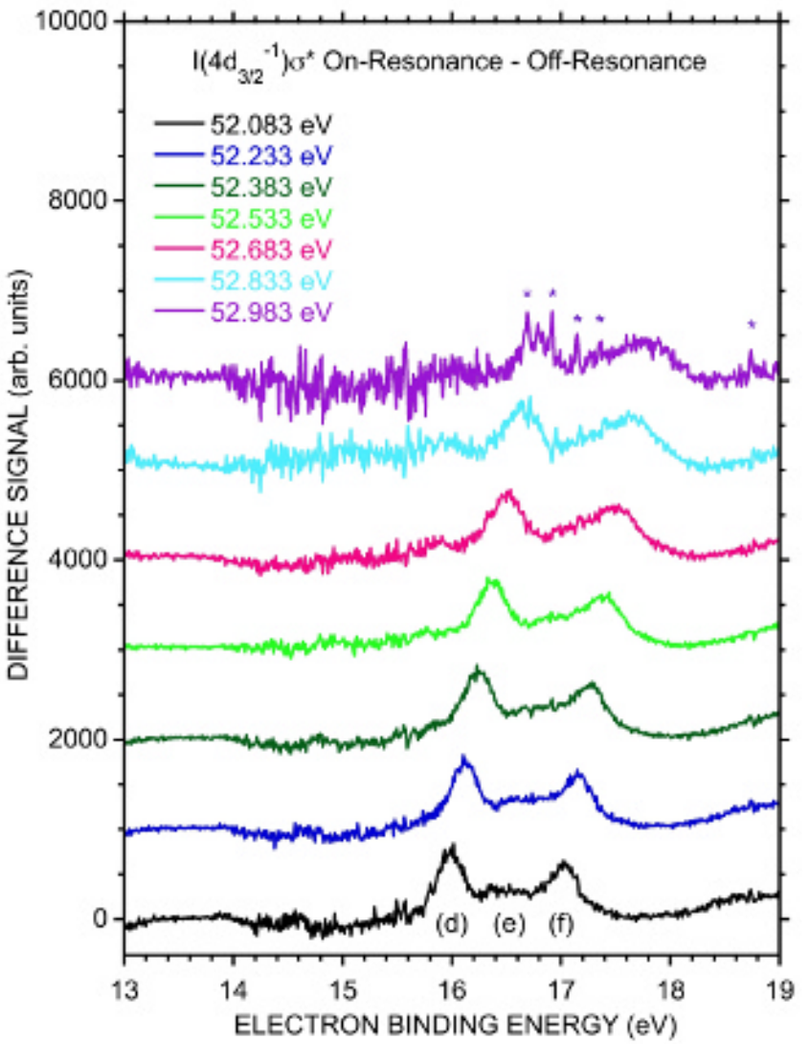

Figure 11. A series of difference magic-angle photoelectron spectra recorded at several energies across the (I $4d_{3/2}^{-1}$)σ* resonance and using the off-resonance spectrum at 50.224 eV. The spectra have all been scaled to the same peak intensity. A small air leak that increased with time produced a series of sharp peaks from N_2 and O_2. To address this issue, the off-resonance spectrum was constructed from a linear combination of background spectra at 52.083 eV and 53.283 eV recorded before and after the series of on-resonance spectra, respectively. Some of this impurity structure is observed as sharp peaks in the weaker spectra at 52.833 eV and 52.983 eV and labeled with an asterisk, *. The features (d), (e), and (f) are labeled to facilitate comparison with Figure 10.

lower photon energies, there appears to be a third feature, (e), between these two peaks. The slopes for all of the resonances are somewhat less than one, indicating that in the region of C-I bond lengths explored in the process, the potential surfaces for the $(CH_3I^{2+})\sigma^*$ states are not as steep as those for the $(4d^{-1})\sigma^*$ states. If the spectator decay is not instantaneous, the increase in C-I bond length is also expected to access less steep portions of the $(CH_3I^{2+})\sigma^*$ potential.

One somewhat surprising aspect of Figures 10 and 11 is that the decay of the $(4d_{5/2}^{-1})\sigma^*$ resonance appears to populate lower-energy (between 14.5 and 15.9 eV) levels of CH_3I^+ that do not appear to be present in the $(4d_{3/2}^{-1})\sigma^*$ spectra. In the regular Auger spectrum of CH_3I^+ following 4d ionization,[14] decay of the $4d_{3/2}^{-1}$ states into the lowest lying states of CH_3I^{2+} appears to be a factor

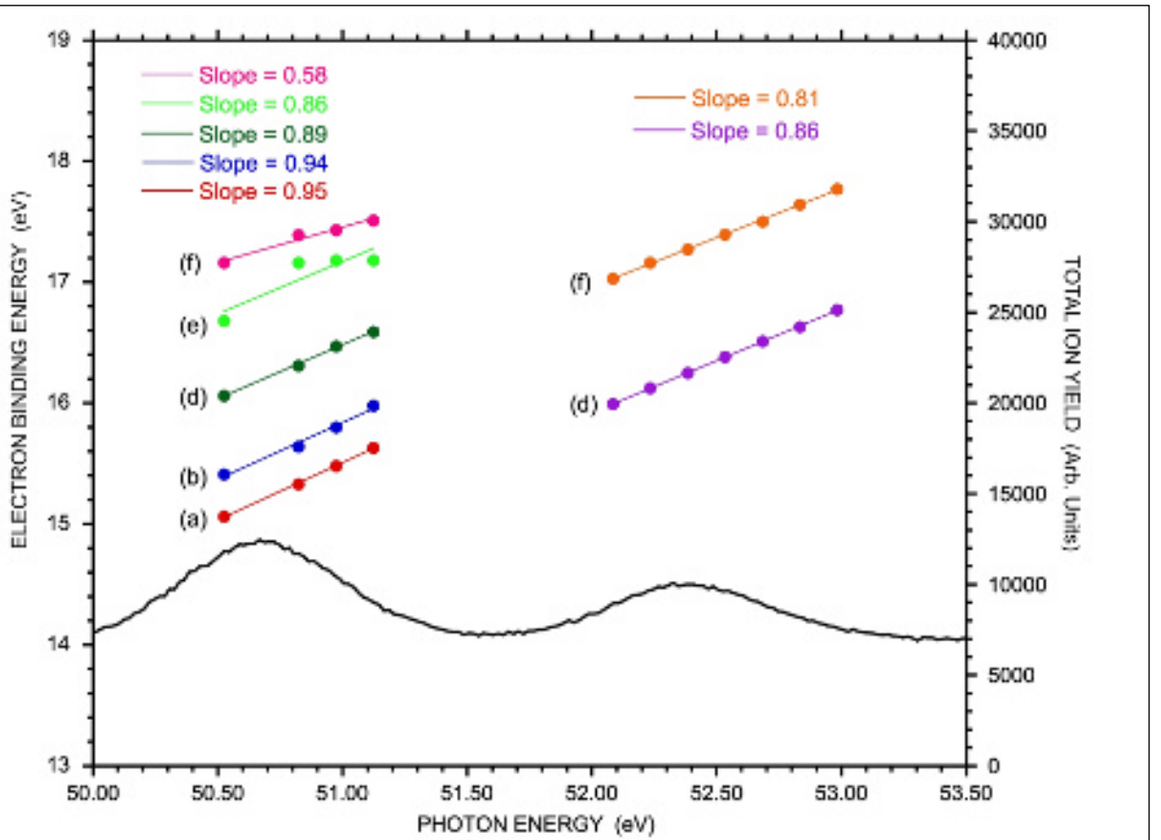

Figure 12. A plot of the total ion yield as a function of photon energy across the $(I\ 4d_{5/2}^{-1})\sigma^*$ and $(I\ 4d_{3/2}^{-1})\sigma^*$ resonances, along with a plots of the peak positions for the spectator decay processes in Figure 10 and 11. The fitted slopes indicate that the kinetic energy of the ejected electron is increasing faster than the photon energy is increasing, indicating the lower states of the spectator processes are not as repulsive as the $(I\ 4d^{-1})\sigma^*$ states.

of ~4 times weaker than for the corresponding $4d_{5/2}^{-1}$ states, and the spectator decay processes may show similar behavior. Nevertheless, even at that intensity, they should still be observable in Figure 11. A second possibility is that the simple subtraction process used to generate Figure 11 breaks down at lower binding energies.

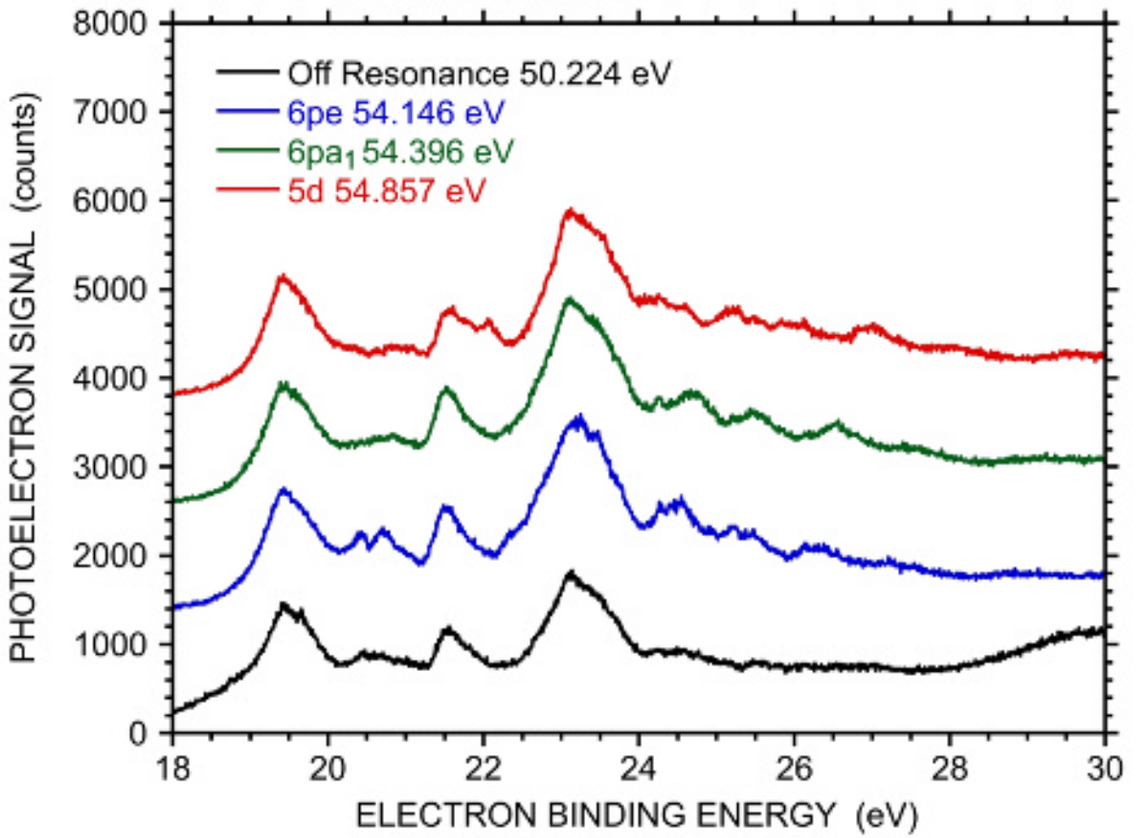

Figure 13. A plot of the spectator Auger spectra for several (I $4d_{5/2}^{-1}$)*nl* resonances in the region just below the I 4d ionization threshold, along with the off-resonance spectrum at 50.224 eV.

C. Spectator Auger Decay to Higher Excited States of CH_3I^+

As can be seen in Figure 4, at electron binding energies above 18 eV there is some evidence for shake-up processes in the spectator decay of the $(4d^{-1})\sigma^*$ resonances, but these features are weak and partially obscured by the other structures in the photoelectron spectra. On the other hand, the principal spectator decay processes for higher energy resonances are expected at higher binding

energies as well. For example, Figure 13 shows a portion of the resonant Auger photoelectron spectra for the $(4d_{5/2}^{-1})6pe$, $(4d_{5/2}^{-1})6pa_1$, and $(4d_{5/2}^{-1})5d$ resonances in Figure 1, along with an off-resonance spectrum at 50.224 eV. The three resonant spectra display no significant additional structure below this energy region, although weak participator decay likely occurs. In contrast, the three resonant processes in Figure 13 show significant new structure not present in the off-resonance spectrum. In particular, the $(4d_{5/2}^{-1})6pe$ decay produces a doublet at 20.43 and 20.71 eV, while the $(4d_{5/2}^{-1})5d$ decay displays a new feature a 22.08 eV. New features associated with $(4d_{5/2}^{-1})6pa_1$ decay may be obscured by some of the larger photoelectron peaks in this region. At higher energies between 24 and 28.5 eV, each of the three resonant spectra in Figure 13 shows a series of new peaks, which have an appearance similar to those for the $(4d^{-1})\sigma^*$ resonances in Figures 10 and 11. These likely access dissociative Rydberg states of CH_3I^+ based on one or more of the low-lying states of CH_3^{2+}.

IV. CONCLUSIONS

This study focuses on participator Auger decay that populates the lowest lying states of CH_3I^+, in particular, the $\tilde{X}\ ^2E_{3/2}$ and $^2E_{1/2}$ states, as well as on spectator decay that populates the lowest-lying $(CH_3I^{2+})\sigma^*$ states of CH_3I^+. Participator decay to the $\tilde{X}\ ^2E_{3/2}$ and $^2E_{1/2}$ states shows a long progression in the ν_3^+ C-I stretching vibration, reflecting decay processes occurring as the C-I bond in the resonantly excited state elongates as the molecule dissociates on the repulsive energy curve of the excited state. In contrast, the spectator Auger decay preferentially populates two-hole, one-particle states of $(CH_3I^{2+})nl$ states on the repulsive walls of the corresponding potentials. Such states tend to display the effects of strong electron correlation and interactions among multiple electronic states. More detailed studies of the spectator decay processes that populate these states, particularly as a function of the character of the initially excited resonances, are expected to provide a much better understanding of these highly correlated states.

Improved calculations of the $(4d^{-1})\sigma^*$ and $(CH_3I^{2+})\sigma^*$ potentials would be helpful for the detailed assignment of the structure in Figures 10 and 11, and in particular, the determination of the final states of the spectator Auger processes. Calculations of the low-lying CH_3I^{2+} potential surfaces along the C-I stretching coordinate would also be helpful. Furthermore, because the dissociative curves of CH_3I^+ between 15 and 19 eV result in several different sets of dissociation products, coincidence measurements of the fragmentation products[56] and their kinetic energies for the different features in Figure 10 would also provide considerable insight into these assignments.

V. SUPPLEMENTAL MATERIAL

The supplemental material provides information on the expected photoelectron energies for autoionization of atomic iodine formed by ultrafast dissociation, along with experimental data showing the absence of features at these expected energies.

VI. ACKNOWLEDGEMENTS

We would like to thank Professor Luis Bañares for providing the potential curves from Reference 39 in digital form, and for providing a preprint of Reference 40. We are grateful to the SOLEIL staff for running the facility and providing beamtime under Project No. 20200370. S.T.P. is supported by the U.S. Department of Energy, Office of Science, Office of Basic Energy Sciences, Division of Chemical Sciences, Geosciences, and Biosciences under contract No. DE-AC02-06CH11357. D.M.P.H. is grateful to the Science and Technology Facilities Council (United Kingdom) for financial support.

REFERENCE

1. V. Schmidt, Electron Spectrometry of Atoms using Synchrotron Radiation (Cambridge University Press, Cambridge, U.K., 1997).
2. G. B. Armen, H. Aksela, T. Åberg, and S. Aksela, The resonant Auger effect, J. Phys. B **33**, R49-R92 (2000).
3. P. Morin and C. Miron, Ultrafast dissociation: An unexpected tool for probing molecular dynamics, J. Electron Spectrosc. Rel. Phenom. **185**, 259-266 (2012).
4. O. Björneholm, S, Sundin, R. R. T. Marinho, A. Naves de Brito, G. Gel'mukhanov, and H. Ågren, Femtosecond dissociation of core-excited HCl monitored by frequency detuning, Phys. Rev. Lett. **79**, 3150-3153 (1997).
5. P. Morin, M. Simon, C. Miron, N. Leclercq, E. Kukk, J. D. Bozek, and N. Berrah, Role of bending in the dissociation of selective resonant inner-shell excitation as observed in CO_2, Phys., Rev. A **61**, 050701(R), 2000.
6. I. Hjelte, M. N. Piancastelli, R. F. Fink, O. Björnholm, M. Bässler, R. Feifel, A. Giertz, H. Wang, K. Wiesner A. Ausmees, C. Miron S. L. Sorensen, and S. Svensson, Evidence for ultra-fast dissociation of water from resonant Auger spectroscopy, Chem. Phys. Lett. **334**, 151-158 (2001).
7. C. Miron, R. Feifel, O. Björneholm, S. Svensson, A. Naves de Brito, S. L. Sorenson, M. N. Piancastelli, M. Simon, and P. Morin, Mapping potential energy surfaces by core electron excitation: the resonant Auger decay spectrum of BF_3, Chem. Phys. Lett, **359**, 48-54 (2002).
8. O. Travnikova, E. Kukk, F. Hosseini, S. Granroth, E. Itälä, T. Marchenko, R. Guillemin, I. Ismail, R. Moussaoui, L. Journel, J. D. Bozek, R. Püttner, P. Krasnov, V. Kimberg, F. Gel'mukhanov, M. N. Piancastelli, and M. Simon, Ultrafast dissociation of ammonia: Auger Doppler effect and redistribution of the internal energy, Phys. Chem. Chem. Phys. **24**, 5842-5854 (2022).

9. O. Travnikova, F. Hosseini, T. Marchenko, R. Guillemin, I. Ismail, R. Moussaoui, L. Journel, A. Milosavljevic, J. D. Bozek, E. Kukk, R. Püttner, M. N. Piancastelli, and M. Simon, Dynamics of core-excited ammonia: disentangling fragmentation pathways by complementary spectroscopic methods, Phys. Chem. Chem. Phys. **25**, 1063-1074 (2023).
10. H. Ågren, J. Nordgren, L. Selander, C. Nordling, and K. Siegbahn, Valence electron structure of the SF_6 and CS_2 molecules, studied by high resolution x-ray emission, Phys. Scripta **18**, 499-505 (1978).
11. P. Morin and I. Nenner, Atomic autoionization following very fast dissociation of core-excited HBr, Phys. Rev. Lett. **56**, 1913-1916 (1986).
12. E. Kukk, H. Aksela, O. -P. Sairanen, E. Nõmmiste, S. Aksela, S. J. Osborne, A. Ausmees, and S. Svensson, Core-to-Rydberg excitations and their Auger decay in the HCl and DCl molecules, Phys. Rev. A **54**, 2121-2126 (1996).
13. O. Travnikova N. Sisourat, T. Marchenko, G. Goldsztejn, R Guillemin, L. Journel, D. Céolin, I. Ismail, A. F. Lago, R. Püttner, M. N. Piancastelli, and M. Simon, Subfemtosecond control of molecular fragmentation by hard x-ray photons, Phys. Rev. Lett. **118**, 213001 (2017).
14. R. Forbes, A. De Fanis, D. Rolles, S. T. Pratt, I. Powis, N. A. Besley, A. R. Milosavljević, C. Nicholas, J. D. Bozek, and D. M. P. Holland, Photoionization of the I 4d and valence orbitals of methyl iodide, J. Phys, B **53**, 155101 (2020).
15. F. Markel and A. B. Myers, Resonance Raman spectra of photodissociating CH_3I and CD_3I in solution, Chem. Phys. Lett, **167**, 175-182 (1990)
16. M. Shapiro, Photophysics of dissociating CH_3I: resonance-Raman and vibronic photofragmentation maps, J. Phys. Chem. **90**, 3644-3653 (1986).
17. A. Strobel, I. Fischer, A. Lochschmidt, K. Müller-Dethlefs, and V. Bondybey, Photodissociation dynamics of CH_3I and CD_3I probed by zero kinetic energy photoelectron spectroscopy, J. Phys. Chem. **98**, 2024-2032 (1994).

18. A. R. Attar, A. Bhattacherjee, and S. R. Leone, Direct observation of the transition state region in the photodissociation of CH_3I by femtosecond extreme ultraviolet transient absorption spectroscopy, J. Phys. Chem. Lett. **6**, 5072-5077 (2015).
19. K. F. Chang, H. Wang, S. M. Poullain, D. Prendergast, D. M. Neumark, and S. R. Leone, Mapping wave packet bifurcation at a conical intersection in CH_3I by attosecond XUV transient absorption spectroscopy, J. Chem. Phys. **154**, 234301 (2021).
20. F. Braußе, G. Goldsztejn, K. Amini R. Boll. S. Bari, C. Bomme, M Brouard, M. Burt, B. Cunha de Miranda, S. Düsterer, B Erk, M. Géléoc, R. Geneaux, A. S. Gentleman, J. Küpper, P. Lablanquie, J. Lahl. J. W. L. Lee, S. R. Mackenzie, S. Maclot, B. Manschwetus, A. S. Mereshchenko, T. Mullins, P O. Olshin, J. Palaudoux, S. Patchovskii, F. Penent, M. N. Piancastelli, D. Rompotis, T. Ruchon, A. Rudenko, E. Savelyev, N. Schirmel, S. Techert, O. Travnikova, S. Trippel, J. G. Underwood, C. Vallance, J Wiese, M. Simon, D. M. P. Holland, T. Marchenko, A. Rouzée, and D. Rolles, Time-resolved inner-shell photoelectron spectroscopy: From a bound molecule to an isolated atom, Phys. Rev. A **97**, 043429 (2018).
21. J. Söderström, A. Lindblad, A. N. Grum-Grzhimailo, O. Travnikova, C. Nicolas, S. Svensson, and C. Miron, Angle-resolved electron spectroscopy of the resonant Auger decay in xenon with meV energy resolution, New J. Phys. **13**, 073014 (2011).
22. K. Codling, R. P. Madden, and D. L. Ederer, Resonances in the photo-ionization continuum of Ne I (20-150 eV), Phys. Rev. **155**, 26-37 (1967).
23. K. Schultz, M. Domke, R. Püttner, A. Gutiérrez, G. Kaindl, G. Miecznik, and C. H. Greene, High-resolution experimental and theoretical study of singly and doubly excited resonances in ground-state photoionization of neon, Phys. Rev. A **54**, 3095-3112 (1996).
24. M. Grütter, J. M. Michaud, and F. Merkt, Photoelectron spectroscopic study of the E⊗e Jahn–Teller effect in the presence of a tunable spin–orbit interaction. I. Photoionization dynamics of methyl iodide and rotational fine structure of CH_3I^+ and CD_3I^+, J. Chem. Phys. **134**, 054308 (2011).

25. C. N. Yang, On the Angular Distribution in Nuclear Reactions and Coincidence Measurements, Phys. Rev. **74**, 764-772 (1948).
26. J. Cooper and R. N. Zare, Angular distribution of photoelectrons, J. Chem. Phys. **48**, 942-943 (1968).
27. K. Reid, Photoelectron Angular Distributions, Ann. Rev. Phys. Chem. **54**, 397-424 (2003).
28. I. Powis, D. M. P. Holland, E. Antonsson, M. Patanen, C. Nicolas, C. Miron, M. Schneider, D. Yu. Soshnikov, A. Dreuw, and A. B. Trofimov, The influence of the bromine atom Cooper minimum on the photoelectron angular distributions and branching ratios of the four outermost bands of bromobenzene, J. Chem. Phys. **143**, 144304 (2015).
29. T. A. Carlson, A. Fahlman, M. O. Krause, P. R. Keller, J. W. Taylor, T. Whitley, and F. A. Grimm, Angle resolved photoelectron spectroscopy of the valence shells in HI and CH_3I as a function of photon energy from 13 to 90 eV, J. Chem. Phys. **80**, 3521-3527 (1984).
30. J. N. Cutler, G. M. Bancroft, and K. H. Tan, Ligand-field splittings and core-level linewidths in I 4d photoelectron spectra of iodine molecules, J. Chem. Phys. **97**, 7932-7943 (1992).
31. See, for example, M. N. Piancastelli, Auger resonant Raman studies of atoms and molecules, J. Electron Spectrosc. Rel. Phenom. **107**, 1-26 (2000).
32. A. Pilcher-Clayton and J. H. D. Eland, Double photoionization spectra of HI, CH_3I, and CH_3I from TOF-PEPECO experiments, J. Electron Spectrosc. Rel. Phenom. **142**, 313-317 (2005).
33. J. H. D. Eland and R. Feifel, *Double Photoionisation Spectra of Molecules* (Oxford University Press, Oxford, UK, 2018).
34. A. Hult-Roos, J. H. D. Eland, D. Koulentianos, R. J. Squibb, L. Karlsson, and R. Feifel, Valence double ionization electron spectra of CH_3F, CH_3Cl, and CH_3I, Chem. Phys. 49, 42-47 (2017).

35. M. Pernpointner, J. P. Zobel, E. Fasshauer, and A N. Sil, Spin-orbit effects, electronic decay and breakdown phenomena in the photoelectron spectra of iodomethane, Chem. Phys. **407**, 39-45 (2012).
36. L. Karlsson, R. Jadrny, L. Mattsson, F.T. Chau, K. Siegbahn, Vibrational and vibronic structure in the valence electron spectra of CH_3X molecules (X = F, Cl, Br, I, OH), Phys. Scripta **16**, 225-234 (1977).
37. K. Kimura, S. Kasumata, Y. Achiba, T. Yamazaki, and S. Iwata, *Handbook of He I Photoelectron Spectra of Fundamental Organic Molecules* (Halsted Press, New York, 1981).
38. H. Lefebvre-Brion and R. W. Field, The Spectra and Dynamics of Diatomic Molecules (Elsevier, Amsterdam, 2004).
39. L. Murillo-Sánchez, G. Reitsma, S. M. Poullain, P. Fernández-Milán, J. González-Vázquez, R. de Nalda, F. Martin, M. J. J. Vrakking, O. Kornilov, and L. Bañares, Femtosecond XUV-IR induced photodynamics in the methyl iodide cation, New J. Phys. **23**, 073023 (2021).
40. See, also: J. González-Vázquez, G. A. Garcia, D. V. Chicarro, L. Bañares, and S. Marggi Poullain, Evidencing an elusive conical intersection in the dissociative photoionization of methyl iodide, Chem. Sci. (in press) DOI: 10.1039/d3sc04065h.
41. B. Ruscic and D. H. Bross, Active Thermochemical Tables (ATcT) values based on ver. 1.122v of the Thermochemical Network, Argonne National Laboratory, Lemont, Illinois 2022; available at ATcT.anl.gov .
42. U. Fano, Effects of configuration interaction on intensities and phase shifts, Phys. Rev. **124**, 1866-1878 (1961).
43. R. Schinke, *Photodissociation Dynamics* (Cambridge University Press, Cambridge, U.K., 1993).
44. M. N. R. Ashfold and J. E. Baggott, Editors, *Molecular Photo-dissociation Dynamics* (Royal Society of Chemistry, London, U.K.,1987).

45. K. Q. Lao, M. D. Person, P. Xayariboun, and L. J. Butler, Evolution of molecular dissociation through an electronic curve crossing: Polarized emission spectroscopy of CH_3I at 266 nm, J. Chem. Phys. **92**, 823-841 (1990).
46. M. Pettini, M. Mazzoni, and G. P. Tozzi, Excitation of the inner 4d shell of neutral iodine, Phys. Lett. **82A**, 168-170 (1981).
47. A. B. Alekseyev, H. -P. Liebermann, R. J. Buenker, and S. N. Yurchenko, J. Chem. Phys. **126**, 234102 (2007).
48. H. Ryufuku, K. Sasaki, and T. Watanabe, Oscillatory behavior of charge transfer cross sections as a function of the charge of particles in low-energy collisions, Phys. Rev. A **21**, 745-750 (1980).
49. A. Niehaus, A classical model for multiple-electron capture in slow collisions of highly charged ions with atoms, J. Phys. B **19**, 2925-2937 (1986).
50. B. Erk, R. Boll, S. Trippel, D. Anielski, L. Foucar, B. Rudek, S. W. Epp, R. Coffee, S. Carron, S. Schorb, K. R. Ferguson, M. Swiggers, J. D. Bozek, M. Simon, T. Warchenko, J. Küpper, I. Schlichting, J. Ullrich, C. Bostedt, D. Rolles, and A. Rudenko, Imaging charge transfer in iodomethane upon x-ray photoabsorption, Science, **345**, 288-291 (2014).
51. R. Boll, B. Erk, R. Coffee, S. Trippel, T. Kierspel, C. Bomme, J. D. Bozek, M. Burkett, S. Carron, K. R. Ferguson, L. Foucar, J. Küpper, T. Marchenko, C. Miron, M. Patenen, T. Osipov, S. Schorb, M. Simon, M. Swiggers, S. Techert, K. Ueda, C. Bostedt, D. Rolles, and A. Rudenko, Charge transfer in dissociating iodomethane and fluoromethane molecules ionizaed by intense femtosecond x-ray pulses, Struct. Dyn. **3**, 043207 (2016).
52. T. F. Gallagher, *Rydberg Atoms* (Cambridge University Press, Cambridge, U.K., 1994).
53. G. Herzberg, *Molecular Spectra and Molecular Structure*, Volume III (Krieger Publishing, Malabar, FL, 1991).
54. B. W. Shore and D. H. Menzel, *Principles of Atomic Spectra* (Wiley, New York, 1960).

55. R. Locht, D. Dehareng, K. Hottmann, H. W. Jochims, H. Baumgärtel, and B. Leyh, The photoionization dynamics of methyl iodide (CH_3I): a joint photoelectron and mass spectrometric investigation, J. Phys. B: At. Mol. Opt. Phys **43**, 105101, 2010.

56. C. Miron and P. Morin, High-resolution inner-shell coincidence spectroscopy, Nucl. Instrum. Meth. Phys. Res. A **604**, 66-77 (2009).